

Design of a Broadband Power Amplifier Based on Power and Efficiency Contour Estimation

Jorge Julian Moreno Rubio¹, Roberto Quaglia², *Member, IEEE*, Alexander Baddeley,
Paul J. Tasker³, *Fellow, IEEE*, and Steve C. Cripps, *Life Fellow, IEEE*

Abstract—This letter presents the design of a broadband power amplifier (PA) that achieves, over the 0.45–3.4-GHz frequency band, an output power between 41.5 and 44.3 dBm and a power added efficiency (PAE) higher than 54%. A four-section transformer has been adopted as the output-matching network in order to target the impedance region defined by a simplified prediction of the power and efficiency contours. The designed PA can find application in flexible hardware for 5G applications, as well as in broadband radar and countermeasure systems.

Index Terms—Broadband matching networks, GaN-based FETs, wideband microwave amplifiers.

I. INTRODUCTION

THE current trend for high-frequency systems in the sub-6-GHz range is seeing an increased demand for flexible radios able to cover very wide ranges of frequencies. Some examples are mobile services in the fifth-generation (5G) networks, radars, and electronic warfare applications. Once again, the power amplifier (PA) is one of the most affected components, since its performance has a significant impact on the overall system, and its design becomes more challenging when targeting very broad-frequency ranges.

Only a few examples of the broadband PAs with an output power higher than 10–15 W are available in the literature (see Table I). Based on the 10-W nominal packaged devices, but still able to exceed that power over the whole bandwidth, the PAs presented in [1]–[3] use different design approaches. The class-J PA design shown in [1] focusses on producing low-pass and bandpass matching design rules for the output matching and the input matching, respectively, which lead to equations for determining the values of the several components. The design in [2] is based on the observation of the optimum load trajectory versus frequency that leads to a simple matching strategy; a real-to-real impedance transformation, followed by the use of a short stub for allowing

Manuscript received April 23, 2020; revised May 29, 2020; accepted June 24, 2020. Date of publication July 13, 2020; date of current version August 7, 2020. This work was supported by the European Union's Horizon 2020 Research and Innovation Programme through the Marie Skłodowska-Curie Agreement under Grant 793529. (*Corresponding author: Jorge Julian Moreno Rubio.*)

Jorge Julian Moreno Rubio is with the Center for High Frequency Engineering, Cardiff University, Cardiff CF24 3AA, U.K., and also with GINTEL, Universidad Pedagógica y Tecnológica de Colombia, Sogamoso 150003, Colombia (e-mail: morenorubioj@cardiff.ac.uk).

Roberto Quaglia, Alexander Baddeley, Paul J. Tasker, and Steve C. Cripps are with the Center for High Frequency Engineering, Cardiff University, Cardiff CF24 3AA, U.K.

Color versions of one or more of the figures in this letter are available online at <http://ieeexplore.ieee.org>.

Digital Object Identifier 10.1109/LMWC.2020.3005833

TABLE I

SUMMARY OF WIDEBAND PAs WITH >10-W OUTPUT POWER

Ref.	BW (GHz)	BW (%)	Gain (dB)	P _{OUT} (W)	PAE (%)
[1]	2–3	40	11.5–12.5	≥10	58–72
[2]	0.6–3.8	145.5	9–14	10–15.5	46–75
[3]	0.4–3	152.9	10–12	10–17.8	53–72
[4]	1.8–2.7	40	≥8	16–29	48–65.2
[5]	0.85–5.4	145.6	8–9.5	22.4–31.6	45–55
This work	0.45–3.4	153.2	8–10.5	14.1–26.9	54–70.4

a proper amount of reactive impedance. The design in [3] uses an optimization algorithm able to optimize the values and to a certain degree also the topology of a matching network based on the L-sections. The topology optimization is enabled by virtual switches that change between the open- and short-circuit stubs.

For a higher output power, 25-W packaged devices have been used in [4] and [5]. In [4], a class-E PA has been designed starting from a systematic comparison of different lumped element matching network topologies. A fourth-order low-pass topology has been selected for the prototype and fabricated using the lumped components. In [5], the source-/load-pull simulations are used to identify the optimum impedance regions, followed by an optimization algorithm for the matching network design based on a figure of merit that automatically leads to the in-band equalization of performance.

This letter also uses a 25-W packaged device for the prototype design. Different from other examples, it adopts a simplified prediction of power and efficiency contours, which can be derived from an observation of the knee profile of the device. A multisection real-to-real transformer is then adopted to synthesize the loads over the target frequency band, with the drain stub adjusting the low-frequency response. The measurements demonstrate an ultraoctave high-efficiency PA, with 153.2% of fractional bandwidth and power added efficiency (PAE) from 54% to 70.4%, for an output power between 14.1 and 26.9 W.

II. DESIGN

The proposed design process starts with a prediction of the load impedance regions with good power and efficiency performance. In [6], a simplified approach for the saturated contour prediction, at the intrinsic generator plane, was presented. In particular, it was based on the observation that the output characteristics (pulsed or RF using fan diagrams) of the device knee can be fit with an output current profile

$$I_D = I_{MAX} [1 - (1 - v_{DS})^N] \quad (1)$$

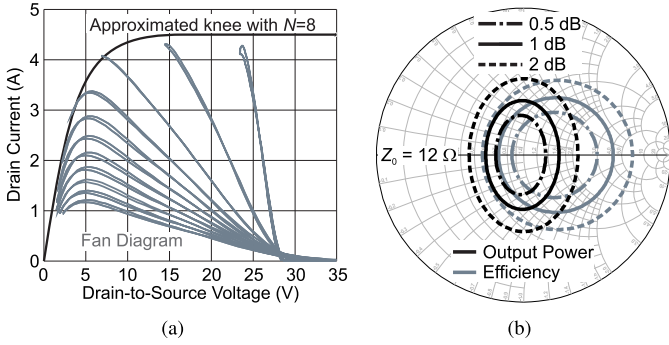


Fig. 1. (a) Fan diagram for the CGH40025 with approximated current profile. (b) Normalized output power and efficiency contours based on [6].

where v_{DS} is the output voltage normalized to the drain bias voltage V_{DD} and I_{MAX} is the maximum device current. N is the key parameter that determines the softness of the knee profile and the only parameter needed to draw the normalized output power and efficiency contours at saturation. In order to denormalize the contours, the ideal optimum load $R_{opt} = 2V_{DD}/I_{MAX}$ must be used. In [6], the contours were verified by means of load-pull characterization, but no PA design was shown using the method proposed.

The device selected for the design is the CGH40025 from Wolfspeed. By observing its output characteristics [see the simulated fan diagram in Fig. 1(a) at 10 MHz], it is possible to approximate the knee profile with $N = 8$, $I_{MAX} = 4.5$ A, and $V_{DD} = 28$ V ($R_{opt} \approx 12 \Omega$). Fig. 1(b) reports the normalized output power (black ellipses) and efficiency (gray circles) contours whose geometrical parameters are reported in [6, Table 1]. In [6], Fig. 6(a) shows the expected maximum output power and efficiency when accounting for the knee. In our case, for $N = 8$, the maximum output power is expected to be $0.18V_{DD}I_{MAX} = 43.6$ dBm, while the maximum efficiency is 68%.

The next step is to account for the frequency dispersion introduced by the device-reactive effects, such as intrinsic capacitance and parasitics. The approach followed has been to use the cold-FET simulations to estimate an equivalent output circuit. In particular, a shunt capacitance of 2.8 pF and a series inductance of 0.37 nH have been considered for this device. The nonlinear effects of the output capacitance have been deemed as secondary and not included, since the goal is to provide a simplified equation and not an accurate large signal model of the device as, for example, proposed in [7]. The normalized contours are denormalized to R_{OPT} and then embedded to the package plane. The proposed method is based on the observation of the power and efficiency contours that then become the target for the design of the output-matching network (OMN). In particular, by choosing an output power contour at 1 dB from the maximum power (centered in -0.01 , normalized ellipse with x -radii of 0.25 and y -radii of 0.37), the resulting contours are shown in Fig. 2(a). On the other hand, Fig. 2(b) reports the efficiency contours also at 1 dB from the maximum efficiency (equivalent to a 0.79 reduction), which are predicted, in normalized form, as a circle centered in 0.22 and with a radius of 0.39. For this particular device, the key observation made is that the real impedance of 12Ω ,

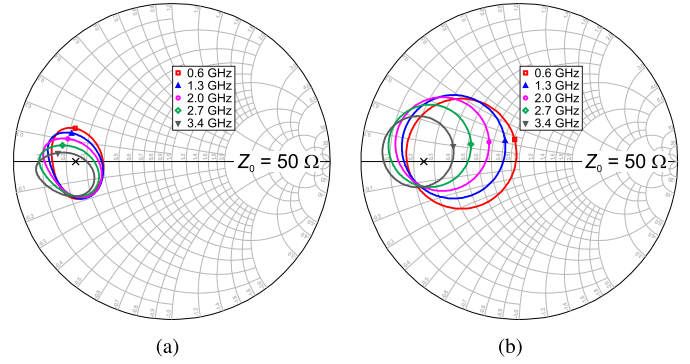


Fig. 2. (a) Estimated power and (b) efficiency 1-dB contours at the package plane for the CGH40025, at different frequencies.

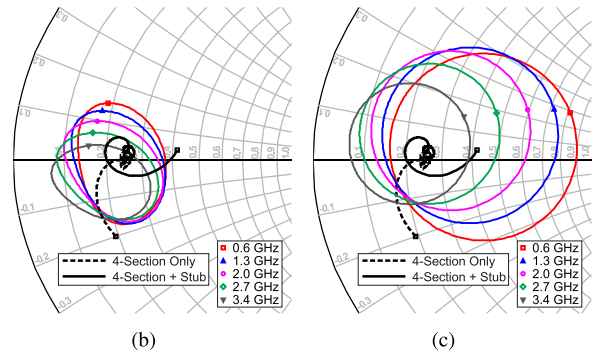
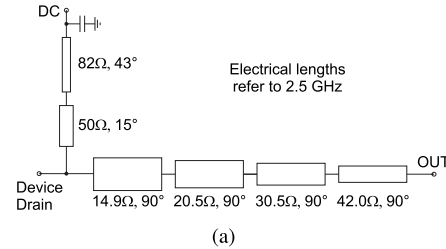


Fig. 3. (a) Ideal schematic of the OMN. Load synthesized by the OMN (black) superimposed over (b) 1-dB power and (c) efficiency contours.

indicated by the black cross in both Smith Charts, can be used as the target for a real-to-real transformation from 50Ω , since it sits within the intersections of both output power and efficiency contours. Therefore, on the target band, the expected output power and efficiency are higher than their maximum minus 1 dB, i.e., 42.6 dBm and 54%, respectively.

The OMN is hence based on a real-to-real impedance transformer that is conveniently realized, in distributed form, with a multisection quarter-wave transformer. Multisection transformers have been used recently in other PA designs, for example, in the postmatching of the Doherty reported in [8]. For this design, the OMN uses a four-section transformer based on a Chebyshev response centered at 2.5 GHz and with a maximum in-band reflection of 0.05. The OMN is completed by a stub for providing the drain bias [see the ideal schematic in Fig. 3(a)]. The role of the stub can be observed by analyzing the synthesized load trajectories before and after inserting the stub (see Fig. 3). Without the stub (dotted trajectory), the low-frequency end of the trajectory is quite close to the power contours but falls away from the efficiency contours. On the other hand, when using the stub, the trajectory is brought back within the efficiency contours and maintained close to the

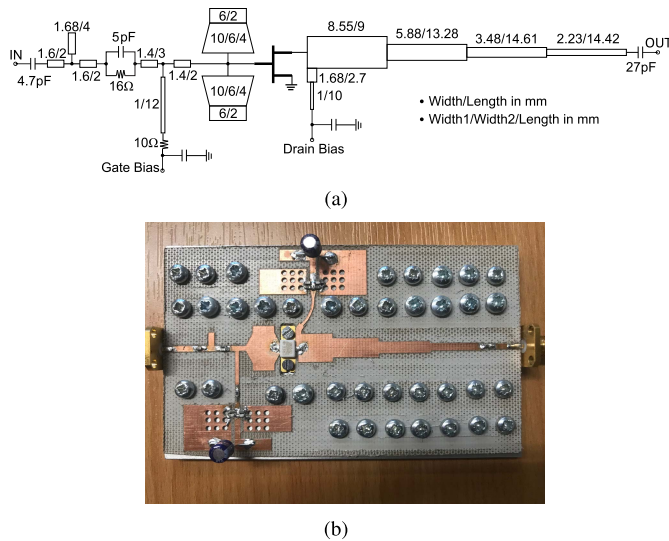


Fig. 4. (a) Full schematic and (b) picture of the realized wideband PA. Size: $69 \times 40 \text{ mm}^2$.

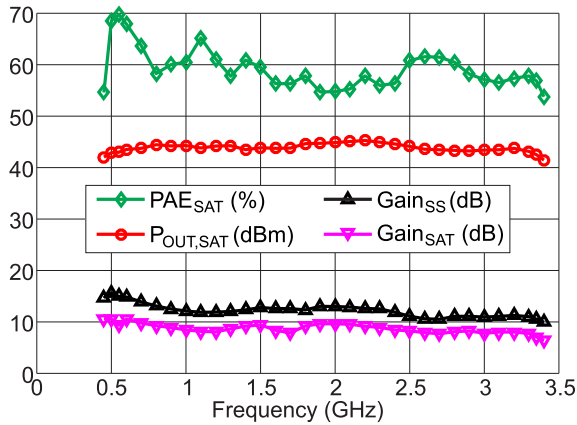


Fig. 5. Measured CW results versus frequency. The index “SAT” refers to saturated condition, while “SS” refers to small signal.

power contour. The second-harmonic load was observed during the design process to avoid resonances, especially above 3.5 GHz where the second harmonic could be potentially tuned. However, it was not tuned, since the device model used was too simplified for any harmonic tuning to make sense.

III. REALIZATION AND CHARACTERIZATION

The complete PA schematic is illustrated in Fig. 4(a). The designed PA is fabricated on a 0.76-mm RF35 Taconic substrate. The input network uses two low-impedance open stubs connected directly to the gate pin for broadband matching. Broadband stabilization is achieved thanks to a series RC network and a resistor on the gate bias path. Both input matching and stability are studied using the scattering parameters. Fig. 4(b) shows a picture of the realized ultrawideband PA. For characterization, the bias current is set at 250 mA (deep class AB) to keep good linearity conditions.

The results in terms of output power, PAE, and gain over the band are shown in Fig. 5. Over a fractional bandwidth of 153% (0.45–3.4 GHz), the measurements show a PAE between 54% and 70.4% and an output power higher than 41.5 dBm. From 0.6 to 3.4 GHz, the output power is higher than 42.6 dBm and

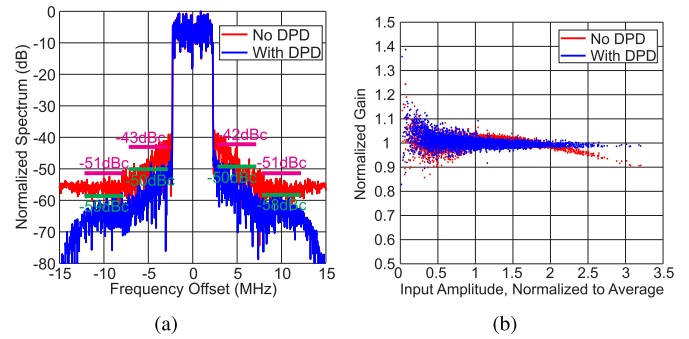


Fig. 6. System-level measurements of the PA at 0.7 GHz. (a) Output spectra and (b) gain, before (red) and after (blue) applying DPD. The average output power is 33.7 dBm in both cases, with an average PAE of 24%.

the efficiency well above 54%, as expected from the simplified theory.

The linearity of the PA has been tested using an OFDM signal with a 9.5-dB peak-to-average ratio at a few different frequencies. Fig. 6 shows the resulting output spectra with an adjacent channel leakage ratio (ACLR) and a gain response at 0.7 GHz, with the corresponding average output power and efficiency. Measurements before digital predistortion (DPD) already show a rather good linearity. The simple DPD algorithm, based on a memory polynomial with an odd order of 8 and a memory depth of 2, demonstrated the linearizability according to the ACLR specifications (lower than -45 dBc). Similar results have been found across the design band.

IV. CONCLUSION

An ultraoctave high-efficiency PA has been designed through a simple real-to-real matching strategy. The obtained PAE is shown to be higher than 54% over a 153% fractional bandwidth, with an output power higher than 14.1 W. The design has been based on a simplified prediction of the power and efficiency contours.

REFERENCES

- [1] X. Meng, C. Yu, Y. Liu, and Y. Wu, “Design approach for implementation of class-J broadband power amplifiers using synthesized band-pass and low-pass matching topology,” *IEEE Trans. Microw. Theory Techn.*, vol. 65, no. 12, pp. 4984–4996, Dec. 2017.
- [2] J. J. Moreno Rubio, V. Camarchia, R. Quaglia, E. F. A. Malaver, and M. Pirola, “A 0.6–3.8 GHz GaN power amplifier designed through a simple strategy,” *IEEE Microw. Wireless Compon. Lett.*, vol. 26, no. 6, pp. 446–448, Jun. 2016.
- [3] C. Ma, Y. Liu, W. Pan, and Y. Tang, “0.4–3.0 GHz highly efficient harmonic-tuned power amplifier,” *Electron. Lett.*, vol. 51, no. 23, pp. 1911–1913, May 2015.
- [4] T. Sharma, P. Aflaki, M. Helaloui, and F. M. Ghannouchi, “Broadband GaN class-E power amplifier for load modulated delta sigma and 5G transmitter applications,” *IEEE Access*, vol. 6, pp. 4709–4719, 2018.
- [5] H. T.-A. Nia and V. Nayyeri, “A 0.85–5.4 GHz 25-W GaN power amplifier,” *IEEE Microw. Wireless Compon. Lett.*, vol. 28, no. 3, pp. 251–253, Mar. 2018.
- [6] R. Quaglia, D. J. Sheppard, and S. Cripps, “A reappraisal of optimum output matching conditions in microwave power transistors,” *IEEE Trans. Microw. Theory Techn.*, vol. 65, no. 3, pp. 838–845, Mar. 2017.
- [7] A. Raffo, F. Scappaviva, and G. Vannini, “A new approach to microwave power amplifier design based on the experimental characterization of the intrinsic electron-device load line,” *IEEE Trans. Microw. Theory Techn.*, vol. 57, no. 7, pp. 1743–1752, Jul. 2009.
- [8] S. Rafati, V. Nayyeri, and M. Soleimani, “A 100-W Doherty power amplifier with super-octave bandwidth,” *IEEE Trans. Circuits Syst. II, Exp. Briefs*, vol. 67, no. 6, pp. 1009–1013, Jun. 2020, doi: 10.1109/TCSII.2019.2929306.